Appl. Phys. B (2013) 113:581–587
DOI 10.1007/s00340-013-5513-3

Applied Physics B
Lasers and Optics

Silver nanoparticle size–dependent measurement of quantum efficiency of Rhodamine 6G

N. Shemeena Basheer · B. Rajesh Kumar · Achamma Kurian · Sajan D. George

Received: 15 April 2013 / Accepted: 8 May 2013 / Published online: 29 May 2013

Abstract The plasmonic absorption band of silver nanoparticles in the visible range of electromagnetic spectrum has been successfully exploited to alter the emission characteristics of the Rhodamine 6G dye molecule. The influence of the nanoparticle size on the fluorescence quantum yield of Rhodamine 6G is interrogated via steady state fluorescence as well as dual beam thermal lens technique. The potential of the thermal lens technique that probe nonradiative path in contrast to radiative path exhibited in the fluorescence spectra as a complementary method to measure the quantum yield of a dye molecule is exploited. Analysis of the results clearly indicates that the particle size and the spectral overlap between the emission spectra of Rhodamine 6G, and absorption spectra of the silver nanoparticles determine the quantum yield value of dye–nanoparticle mixture.

1 Introduction

Fluorescence quantum yield, a measure of conversion efficiency of absorbed photons into emitted photons, is one of the fundamental properties of emitters such as organic dyes, quantum dots etc. [1–3]. The fluorescence of an emitter can be tailored when the fluorophore placed in the vicinity of an entity possessing an electromagnetic (plasmon) field [4]. Recently, metal nanoparticles (NPs) that exhibit plasmonic absorption band in the visible range have been employed to tailor the fluorescence quantum yield of the dye molecules via plasmonic field created by the particle [5, 6]. In close proximity of a nanoparticle, depending upon the dye-nanoparticle distance, the fluorescence emission efficiency of a dye molecule can either be enhanced or decreased [7, 8]. The plasmonic field generated around the particle by the incident light can increase excitation decay rate of the fluorophore which in turn enhances the level of fluorescence emission. On the other hand, the dipole energy around the nanoparticle reduces the ratio of the radiative to nonradiative decay rate and the quantum yield of the fluorophore, resulting in fluorescence quenching. In general, the energy transfer efficiency between the NP and the dye molecule depends upon three factors (i) Coulombic spectral overlap integral (ii) The position of the absorption spectrum of the nanoparticle (surface plasmon frequency) and (iii) Width of the absorption spectrum (inverse of plasmon life time). However, for a given metal NP, the plasmonic absorption band normally lies in the visible wavelength range of the electromagnetic spectrum, and it is a function of particle size and shape. As a consequence, the size of the NP can be used to tailor the emission behavior of a nearby dye molecule. Normally, the energy transfer mechanism between the dye molecule and NP can be either radiative or nonradiative. The radiative energy transfer involves the emission of photon by the emitter and subsequent re-absorption by the absorber. The efficient and rapid nonradiative energy transfer occurs via dipole–nanoparticle interaction. Recent studies showed that, compared to dipole–dipole interaction based on Forster resonance energy transfer mechanism that follows R^{-6} dependence for the emitter-acceptor distance, dipole—metal surface-based nanometal surface energy transfer mechanism that follows R^{-4} scaling

N. S. Basheer · B. R. Kumar · A. Kurian
Photonics Research Lab, Department of Physics, Catholicate College, Pathanamthitta 689645, India

S. D. George (✉)
Center for Atomic and Molecular Physics, Manipal University, Manipal 576104, Karnataka, India
e-mail: sajan.george@manipal.edu

is more appropriate in explaining energy transfer mechanism between dye and NP mixtures [9–11]. In general, for large NPs (a $\sim$ 7 nm), the plasmon frequencies can be considered to be independent of particle size. In such cases, the energy transfer rate is mainly determined by the coulombic interactions and the spectral overlap between the plasmonic absorption band and the emission band of the dye molecule. In this work, the dependence of silver NP (Ag NP) sizes of the range between 12 and 31 nm on the quantum yield of Rhodamine 6G (Rh 6G) using dual beam thermal lens technique is investigated.

Thermal lens (TL) technique is a photothermal technique that indirectly measure the fraction of the incident radiant power converted into heat [12, 13]. In TL technique, the absorption of Gaussian laser beam inside the medium causes excitation of ground state molecules. The nonradiative relaxation processes increases the local temperature, creating a refractive index gradient in the sample and inducing an optical lens, the so-called thermal lens. The nature of TL created depends on the temperature coefficient of refractive index of the sample and in most of the materials, it is a diverging one. The time-dependent thermal lens signal is measured by the fractional change in the detected power at the center of the beam at the far field, which is dependent on factors such as sample concentration, sample position, power of the pump laser beam etc. In addition to being a complementary approach to conventional fluorescence technique, the TL technique offer the advantage of direct probing of nonradiative path of de-excitation of the excited molecule. TL technique is successfully employed for the evaluation of quenching efficiency of dye–nano mixtures [11, 14], thermal diffusivity measurement of noble metallic nanofluids, energy transfer study in organic dye mixtures, quantum yield study etc. [15–17].

The present study on Ag NP size-dependent quantum efficiency measurement of Rh 6G is extremely important as Rh 6G is a commonly employed laser medium. Rh 6G–AgNP combination is prominent among various dye–nano mixtures, since Rh 6G is readily adsorbed to AgNP surfaces. It has been reported that in the presence of aggregated Ag NPs, Rh 6G exhibit emission band with a peak wavelength around 612 nm [18]. The aggregated Ag NPs can efficiently act as substrate for surface enhanced Raman spectroscopic studies. It is also reported that Ag NPs can either enhance or decrease the intrinsic fluorescence of Rh 6G depending upon the relative distance between them [19]. This has been exploited in surface enhanced fluorescence studies as well as in many biosensors. The quenching of fluorophore emission may be due to energy transfer [10], electron transfer [20] or by decreasing the radiative rate of the fluorophores [4], and enhancement in emission is attributed to the increase in the radiative rate or absorbance of dye. Researchers carried out detailed studies based on both fluorescence emission and enhancement of Rh 6G on silver island films [21]. It is seen that the fluorescence enhancement depends on the morphology of the substrate surface as well as the distance between fluorophore molecules and the substrate surface. Fluorescence quenching of laser dyes in the presence of AgNPs in different media has also been studied [22]. Owing to the widespread applications, the present study wherein the focus is made on the nonradiative probing of Ag NP size-dependent luminescence behavior of Rh 6G has great physical significance as well as practical importance.

2 Sample preparation

Silver nanofluids of different particle sizes were synthesized using chemical reduction method (citrate-reduction method). Chemical reduction method is adopted for preparation due to high yield, low preparation cost and yielding nanoparticles without agglomeration [23–25]. Silver nitrate ($AgNO_3$) is used as the metal precursor, and sodium citrate tribasic dehydrate ($C_6H_5O_7Na_3$) acts as the reducing agent as well as the stabilizing agent for the preparation of silver nanofluid in double-distilled water. A 250 ml of 1×10^{-3} M silver nitrate solution is heated at 85 °C for several minutes. Then, 5, 10, 20 and 40 ml of 1 % trisodium citrate solution was added drop by drop to this warm solution along with vigorous stirring, to synthesize silver nanoparticles having different particle sizes. The prepared silver nanoparticles are highly stabilized by the repulsive force arising from the negative charge of adsorbed citrate ions. This prevents aggregation of the particles for several weeks. Accurately weighed amount of Rhodamine 6G (donor) is dissolved in double-distilled water to give a concentration of 1×10^{-6} M which is mixed with silver nanofluid having varying particle sizes.

3 Experimental setup

The dual beam TL set up implemented for quantum yield study is given in Fig. 1. A continuous wave diode pumped solid state laser (Coherent Inc., 10 mW) at 532 nm, and a He–Ne laser at 632.8 nm (Melles Griot, 1 mW) are used as the pump and probe beams, respectively, to generate TL in the sample. Collinearity of the pump beam with the probe beam is achieved by utilizing a dichroic mirror. The pump and probe beams are focused at the sample (which is placed one confocal distance past the beam waist) using convex lenses of focal length 40 and 20 cm, respectively. A filter is placed in the path of emergent beams which allows only the probe beam to pass through it. The signal output from the photodetector (PD) is processed using a lock-in

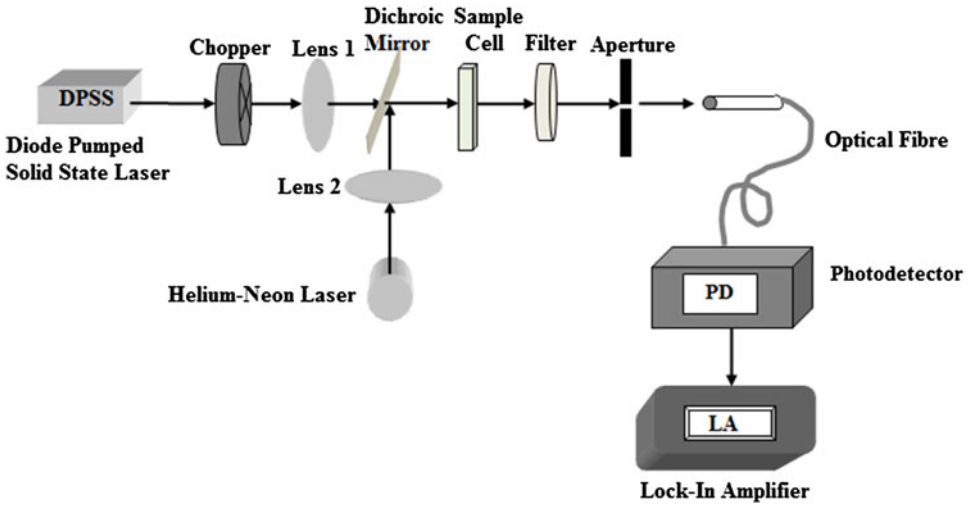

Fig. 1 Experimental setup for quantum yield studies

amplifier (SRS 830). A reference signal is given to the lock-in amplifier using mechanical chopper (Stanford Research Systems SR 540), and the lock-in detection enables yield high signal to noise ratio.

4 Theory

The transition of the molecule from electronically excited singlet state to the ground state resulting in fluorescence emission and the typical emissive rate of such quantum mechanically allowed transitions is about $10^8\ s^{-1}$. The process in which the fluorescence intensity of substance decreases, which assuredly increases the nonradiative transition, gives the way to find out the fluorescence quantum yield values. The method of finding the quantum yield is based on the principle of conservation of energy. If P_0 is the power of the incident pump beam and P_t the power of the transmitted beam, then, the absorbed power is the sum of the power transmitted, thermal power degraded to heat P_{th} and luminescence emission power P_f, provided that there occurs no photochemical reaction.

Hence, we can write

$$P_0 = P_{th} + P_f + P_t \tag{1}$$

where it is assumed that the reflection and scattering losses are negligibly small [26]so that the transmission ratio is given by

$$T = \frac{P_t}{P_0} \tag{2}$$

Absorbance is given by

$$A = 1 - T \tag{3}$$

Thus, the absorbed power is given by

$$AP_0 = P_{th} + P_f \tag{4}$$

Then,

$$P_f = AP_0 - P_{th} \tag{5}$$

In the case of totally fluorescence-quenched sample, we can consider the entire excitation energy to be converted into heat by nonradiative relaxation process. The fluorescence quantum yield Q_f is given by [26].

$$Q_f = \frac{P_f}{AP_0}\frac{\lambda_f}{\lambda} = \left(1 - \frac{P_{th}}{P_\alpha}\right)\frac{\lambda_f}{\lambda} \tag{6}$$

where

$$P_\alpha = AP_0 \tag{7}$$

Here λ_f is the peak fluorescence wavelength, and λ is the excitation wavelength. P_{th} is directly proportional to η, the TL signal measured for each particle size and P_α is proportional to TL signal η_α corresponding to the particle size at which the fluorescence intensity is quenched completely. By knowing λ_f, η and η_α, we can evaluate the quantum efficiency Q_f from the equation given by

$$Q_f = \frac{\lambda_f}{\lambda}\left(1 - \frac{\eta}{\eta_\alpha}\right) \tag{8}$$

The thermal lens signal η has been measured as the variation of intensity at far field at the center of the probe beam arising from thermal lensing effect in the medium.

5 Results and discussions

5.1 Transmission Electron Microscope (TEM) and absorption studies

The size and morphology of silver nanoparticles were determined using transmission electron microscope (HITACHI H-7650). Suspension of the sample were dropped on

formvar grids, dried and viewed under TEM at an accelerating voltage of 80 kV. The morphology of the particles is found to be nearly spherical, and the size of the particles is ranging from 12 nm to 31 nm as shown in Fig. 2a–d, respectively.

The absorption spectra of silver nanofluids are measured using UV–VIS absorption spectrophotometer (SHIMADZU UV-2401 PC) and shown in Fig. 3. The localized surface plasmon resonance (LSPR) wavelengths varied from 428 to 440 nm, and the variation of LSPR wavelength with particle size is shown as inset in Fig. 3. The LSPR absorption band of silver nanoparticles strongly depends upon the particle size, shape, state of agglomeration and the surrounding dielectric media [27–29]. When the particle size is less than mean free path of 'd' electrons in Ag atoms (50 nm), extinction is dominated by absorption rather than scattering. The position of the peak depends upon the dielectric constant of the particle and the surrounding medium. In the case of spherical NPs whose size is within a few percentage of the incident light, a single localized plasmon resonance corresponding to dipolar resonance is observed. In the present case, the particles are nearly spherical, and the red shift can be attributed mainly to the increase in particle size which is consistent with Mie theory [30].

5.2 Fluorescence and thermal lens measurement studies

The fluorescence spectra of Rh 6G alone and the mixture with different particle sizes were taken using the spectrofluorophotometer (SHIMADZU RF-5301 PC) and are shown in Fig. 4. In our studies, 510 nm is used as the excitation wavelength. It is clear from Fig. 4 that the nanoparticles in mixture quench the fluorescence emission of the Rh 6G and quenching efficiency increases with the particle size. This can be attributed to the difference in plasmon field strength around a nanoparticle that influences the fluorescence of the dye molecule. The plasmon field strength around a nanoparticle depends upon its particle size and its strength decreases rapidly with the increase in distance from the surface. For small particles, the field strength decreases rapidly compared to larger particles. Thus, at a given distance from the particle, the

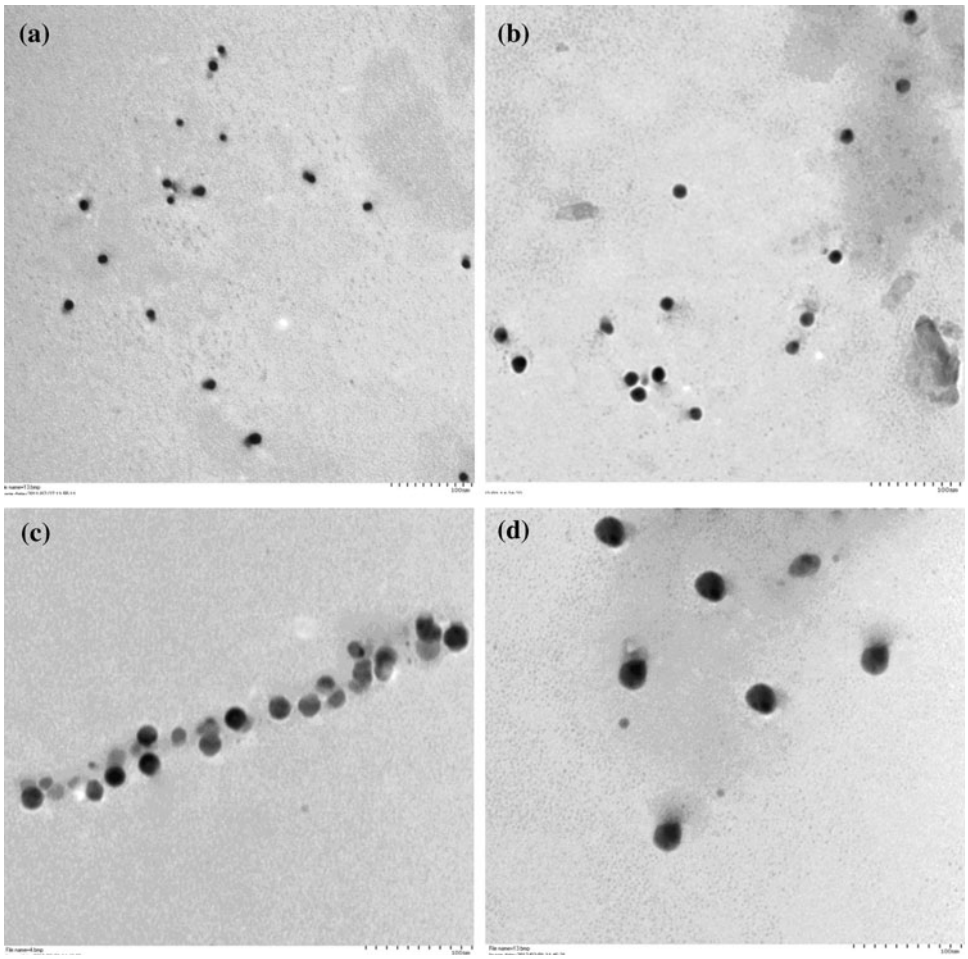

Fig. 2 Transmission Electron Microscope images of silver nanoparticles. **a** 12 nm, **b** 15 nm, **c** 22 nm, and **d** 31 nm

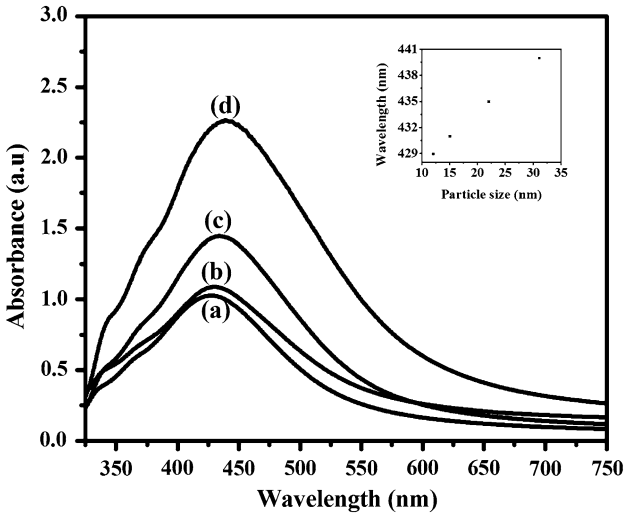

Fig. 3 Absorption spectra of silver nanoparticles. **a** 12 nm, **b** 15 nm, **c** 22 nm and **d** 31 nm (*inset* shows the variation of LSPR wavelength with particle size)

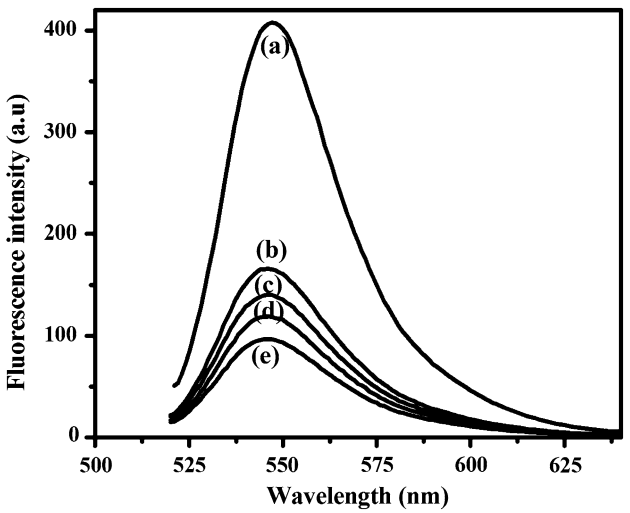

Fig. 4 Fluorescence spectra of Rh 6G–Ag nanoparticle mixture having different particle sizes. **a** Dye alone, **b** 12 nm, **c** 15 nm, **d** 22 nm and **e** 31 nm

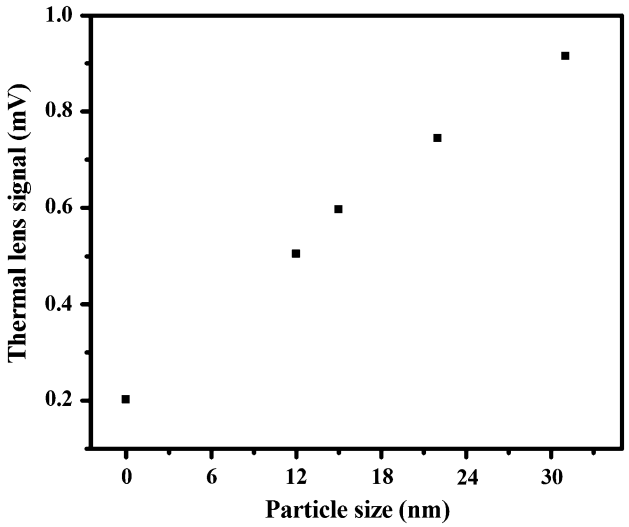

Fig. 5 Thermal lens signal variation of Rh 6G with silver nanoparticle size

interactive field experienced by the dye molecule is smaller for small particle and the corresponding quenching efficiency is smaller. In addition, the increase in absorption coefficient as well as red shift in the plasmon absorption band of the Ag NPs with particle size increases the spectral overlap between emission spectrum of Rh 6G and LSPR band of Ag NPs. This enhanced spectral overlap enables more efficient nonradiative energy transfer and subsequently enhance the quenching of dye molecule fluorescence by the NP. It is also observed that the peak fluorescence emission wavelength of Rh 6G is slightly blue shifted with the addition of nanoparticles. The observed blue shift may be due to the local enhancement of the optical fields near the dye molecules by interactions with silver plasmons.

In order to probe that the fluorescence quenching is happening via nonradiative energy transfer rather than electronic transfer, the thermal lens signal of Rh 6G in the presence and absence of NPs is measured. The variation in thermal lens signal as a function of particle size is shown in Fig. 5. It is observed that in the presence of NPs, the thermal lens signal enhances with NP size. The concentration of Rh 6G employed here is very low so that the possibility of self-quenching by aggregate (H or J type) dimer formation is excluded. Moreover, the NP size dependence of thermal lens signal indicate that spectral overlap between the Rh 6G fluorescence emission spectrum and plasmonic absorption spectrum of the NP is the main contributing factor in determining the experimentally observed fluorescence quenching or enhancement in thermal lens signal. With the increase in particle size, the height and the width of the plasmonic absorption band increases. For particle sizes employed here, the absorption properties of the particles dominate over the scattering. In the proximity of these particles, the dyes transfer their energy nonradiatively to the nanoparticles and exhibit fluorescence quenching or increase in thermal lens signal.

This quenching in fluorescence or increase in thermal lens signal is normally reflected in the fluorescence quantum yield (FYQ) of the dye molecule. Corresponding to each particle size, the FYQ is measured using the Eq. (8) as shown in Fig. 6. The FYQ of the pristine Rh 6G (0.93) agrees well with the earlier reported values [31]. However, the enhanced nonradiative energy transfer with increase in particle size reduces the intrinsic quantum yield of the Rh 6G molecules.

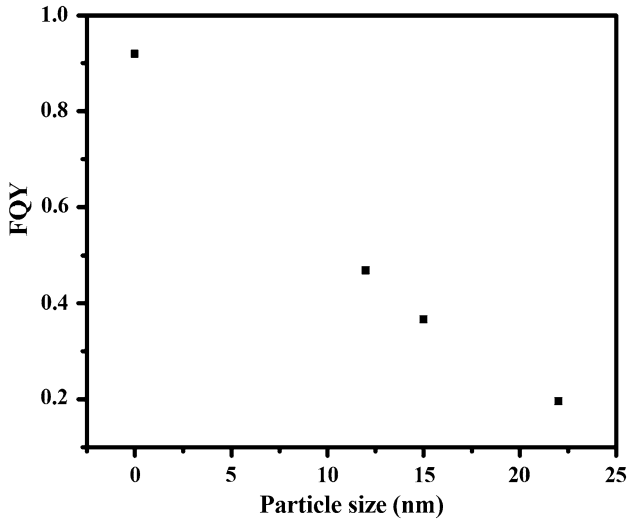

Fig. 6 Variation of quantum yield of Rh 6G versus size of nanoparticle

The quenching efficiency ϕ can be evaluated in terms of thermal lens signal [11, 14] as given below

$$\phi = 1 - \frac{\eta_L^D}{\eta_L^{DA}} \tag{9}$$

where η_L^D and η_L^{DA} are the thermal lens signals measured for the donor alone and with the acceptor, respectively. The quenching efficiency of Rh 6G (1×10^{-6}) M in presence of AgNPs of different sizes 12, 15, 22 and 31 nm is evaluated using Eq. (9). In order to ensure the complementary nature of the TL technique, the efficiencies obtained from the TL method are compared to that from the fluorescence method. The quenching efficiency from the photoluminescence (PL) measurement can be evaluated using the equation

$$\phi = 1 - \frac{F_{DA}}{F_D} \tag{10}$$

where F_D and F_{DA} are the relative fluorescence intensity of the donor in the absence and presence of the acceptor, respectively. The calculated efficiencies using TL and PL method are given in Table 1. From the Table 1, it is clear that the evaluated quenching efficiency values are nearly the same for TL as well as steady state fluorescence technique, indicating the complementary nature of both techniques. Analysis also suggests that the quenching efficiency of Rh 6G increases with increase in AgNP size. The increase in quenching efficiency of Rh 6G with increase in particle size can be understood in terms of more efficient nonradiative energy transfer between the particle and the dye molecule due to enhanced spectral overlap. From the present study, it is evident that there is an increase in quenching efficiency as well as decrease in FQY of Ag NP–Rh 6G mixture with increase in nanoparticle size.

Table 1 Calculated quenching efficiency of Rh 6G for various Ag NP sizes

Particle size (nm)	Φ % TL method	Φ % PL method
12	60.07	59.06
15	66.10	65.44
22	72.88	71.07
31	77.94	76.23

6 Conclusions

It is observed that, in the Rhodamine 6G–Ag nanoparticle mixture, the intrinsic fluorescence of Rh 6G decreases with increase in the particle size due to more efficient spectral overlap between the emitter and absorber. The enhancement of absolute intensity and spectral width of the absorption spectrum of the nanoparticle with increasing size and consequently more efficient spectral overlap enables more efficient nonradiative energy transfer between the nanoparticle and the dye molecule which reflects in corresponding thermal lens as well as static fluorescence signal. Moreover, the quenching efficiency values are measured using both approaches which clearly show that thermal lens technique that probe nonradiative path of de-excitation can be effectively utilized to measure the quantum yield of dye–NP mixtures. Thus, thermal lens technique can be used as an alternate technique where direct fluorescence measurements are practically difficult. This size-dependent increased nonradiative energy transfer between the dye molecule and the nanoparticle can be exploited to develop future biological sensors.

Acknowledgments Authors gratefully acknowledge financial support from the University Grants Commission (UGC), India, through the project F.No.34-31/2008 (SR) dated 20/12/2008.

References

1. K. Rurack, M. Spieles, Anal. Chem. **83**, 1232 (2011)
2. M. Grabolle, M. Spieles, V. Lesnyak, N. Gaponik, A. Eychmüller, U. Resch-Genger, Anal. Chem. **81**, 6285 (2009)
3. U. Resch-Genger, M. Grabolle, S.C. Jaricot, R. Nitschke, T. Nann, Nat. Methods **5**, 763 (2008)
4. E. Dulkeith, A.C. Morteani, T. Niedereichholz, T.A. Klar, J. Feldmann, S.A. Levi, F.C.J.M. van Veggel, D.N. Reinhoudt, M. Moller, D.I. Gittins, Phys. Rev. Lett. **89**, 203002 (2002)
5. G.P. Acuna, M. Bucher, I.H. Stein, C. Steinhauer, A. Kuzyk, P. Holzmeister, R. Schreiber, A. Moroz, F.D. Stefani, T. Liedl, F.C. Simmel, P. Tinnefeld, ACS Nano **6**, 3189 (2012)

6. R. Gill, L. Tian, W.R.C. Somerville, E.C. Le Ru, H. van Amerongen, V. Subramaniam, J. Phys. Chem. C **116**, 16687 (2012)
7. R. Chhabra, J. Sharma, H. Wang, S. Zou, S. Lin, H. Yan, S. Lindsay, Y. Liu, Nanotechnology **20**, 485201 (2009)
8. K.A. Kang, J. Wang, J.B. Jasinski, S. Achilefu, J. Nanobiotechnol. **9**, 1 (2011)
9. T.L. Jennings, M.P. Singh, G.F. Strouse, J. Am. Chem. Soc. **128**, 5462 (2006)
10. C.S. Yun, A. Javier, T.L. Jennings, M. Fisher, S. Hira, S. Peterson, B. Hopkins, N.O. Reich, G.F. Strouse, J. Am. Chem. Soc. **127**, 3115 (2005)
11. N.S. Basheer, B.R. Kumar, A. Kurian, S.D. George, J. Lumin. **137**, 225 (2013)
12. A. Kurian, K.P. Unnikrishnan, S.D. George, P. Gopinath, V.P.N. Nampoori, C.P.G. Vallabhan, Spectrochim. Acta A Mol. Biomol. Spectrosc. **59**, 487 (2003)
13. A. Kurian, S.T. Lee, K.P. Unnikrishnan, S.D. George, V.P.N. Nampoori, C.P.G. Vallabhan, J. Nonlinear Opt, Phys. Mater. **12**, 75 (2003)
14. B.R. Kumar, N.S. Basheer, A. Kurian, S. D. George, *Proceedings of IEEE* 149 (2012)
15. S.A. Joseph, S. Mathew, G. Sharma, M. Hari, A. Kurian, P. Radhakrishnan, V.P.N. Nampoori, Plasmonics **5**, 63 (2010)
16. A. Kurian, S.D. George, V.P.N. Nampoori, C.P.G. Vallabhan, Spectrochim. Acta A Mol. Biomol. Spectrosc. **61**, 2799 (2005)
17. A. Kurian, S.D. George, C.V. Bindhu, V.P.N. Nampoori, C.P.G. Vallabhan, Spectrochim. Acta A Mol. Biomol. Spectrosc. **67**, 678 (2007)
18. M.A. Noginov, M. Vondrova, S.M. Williams, M. Bahoura, V.I. Gavrilenko, S.M. Black, V.P. Drachev, V.M. Shalaev, A. Sykes, J. Opt. A: Pure Appl. Opt. **7**, S219 (2005)
19. S. Kalele, A.C. Deshpande, S.B. Singh, S.K. Kulkarni, Bull. Mater. Sci. **31**, 541 (2008)
20. S.K. Ghosh, A. Pal, S. Kundu, S. Nath, T. Pal, Chem. Phys. Lett. **395**, 366 (2004)
21. G. Liu, H. Zheng, M. Liu, Z. Zhang, J. Dong, X. Yan, X. Li, J. Nanosci. Nanotechnol. **11**, 9523 (2011)
22. Y.S. EI-Syed, M. Gaber, Adv. Nanoparticles **1**, 54 (2012)
23. H.H. Huang, F.Q. Yan, Y.M. Kek, C.H. Chew, G.Q. Xu, W. Ji, P.S. Oh, S.H. Tang, Langmuir **13**, 172 (1997)
24. R. Harpeness, A. Gedanken, Langmuir **20**, 3431 (2004)
25. A. Henglein, J. Phys. Chem. B. **104**, 1206 (2000)
26. A. Santhi, M. Umadevi, V. Ramakrishnan, P. Radhakrishnan, V.P.N. Nampoori, Spectrochim. Acta A Mol. Biomol. Spectrosc. **60**, 1077 (2004)
27. T.R Jensen, M.L. Duval, K.L. Kelly, A.A. Lazarides, G.C. Schatz, R.P. Van Duyne, J. Phys. Chem. B **103**, 9846 (1999)
28. C.L. Haynes, R.P. Van Duyne, J. Phys. Chem. B. **105**, 5599 (2001)
29. K.L. Kelly, E. Coronado, L. Zhao, G.C. Schatz, J. Phys. Chem. B. **107**, 668 (2003)
30. G. Mie, Ann. Phys. **25**, 377 (1908)
31. J. Hung, J. Castillo, A.M. Olaizola, J. Lumin. **101**, 263 (2003)